Article

Not peer-reviewed version

Variations in Ice Discharge and a Frontal Ablation Estimate of Marine-Terminating Glaciers Throughout Alaska from 2015-2021

Hannes Zierer , Dakota Pyles , Thorsten Seehaus *

Posted Date: 10 April 2026

doi: 10.20944/preprints202604.0745.v1

Keywords: ice discharge; frontal ablation; Alaska; marine-terminating glaciers

 doi:10.20944/preprints202604.0745.v1

Article

Variations in Ice Discharge and a Frontal Ablation Estimate of Marine-Terminating Glaciers Throughout Alaska from 2015-2021

Hannes Zierer, Dakota Pyles and Thorsten Seehaus *

Institute of Geography, Friedrich-Alexander-Universität Erlangen-Nürnberg, 91058 Erlangen, Germany

* Correspondence: thorsten.seehaus@fau.de

Abstract

Marine-terminating glaciers are major contributors to sea-level rise, yet their frontal ablation—the combined loss from ice discharge and terminus retreat—remains poorly constrained. This study presents a monthly time series of ice discharge for 40 marine-terminating glaciers in Alaska from 2015 to 2021, derived from Sentinel-1 velocity data, and reconstructed ice thickness information. Frontal ablation was calculated as the sum of ice discharge and terminus mass loss, from manually delineated terminus positions. The mean annual ice discharge was 11.81 ± 5.35 Gt a^{-1}, dominated by Hubbard, Columbia and Yahtse glaciers, which together accounted for ~70% of Alaska's total ice discharge. Terminus retreat contributed an additional 1.30 ± 0.07 Gt a^{-1}, resulting in a total frontal ablation of 13.11 ± 5.35 Gt a^{-1}. Most glaciers exhibited late-summer velocity minima likely indicating seasonal changes in subglacial drainage efficiency, while interannual variability corresponded with El Niño-Southern Oscillation (ENSO) and Pacific Decadal Oscillation (PDO) phases. These findings confirm that Alaska's marine-terminating glaciers currently lose relatively little mass through frontal retreat compared to their regional mass balance, suggesting that most glaciers have passed their phase of rapid retreat. The presented analysis also provides fundamental information for refining sea-level rise projections.

Keywords: ice discharge; frontal ablation; Alaska; marine-terminating glaciers

1. Introduction

Global atmospheric warming has accelerated over the past few decades [1–3]. Mountain regions, which rely on seasonal runoff from snow and glaciers, are particularly affected by warming rates of 0.2 ± 0.1 °C per decade above the global average [4]. Rapid glacier mass loss has been observed outside the Greenland and Antarctic ice sheets [4–7], making glaciers important indicators of climate change [8–10].

Although glaciers hold less than 1% of Earth's land ice [11], they currently contribute 25 - 30% to global sea-level rise (SLR) [6,12]. During the last century, from 1902 to 2009, glaciers have lost 114 ± 5 mm sea-level equivalent (SLE) of mass [13]. Alaska and Arctic Canada have been identified as major contributors to this loss [14,15].

For marine-terminating glaciers, mass balance not only includes surface accumulation and ablation processes but also frontal ablation, which is the mass loss along the glacier terminus due to iceberg calving, submarine melting, and subaerial sublimation [16–18]. Frontal ablation is defined as the sum of ice discharge and terminus mass change due to retreat or advance, and remains one of the least constrained processes in sea-level rise predictions [16,17,19].

Compared to other regions in the Northern Hemisphere, ice discharge was suggested to be the most important driver for frontal ablation in Alaska [19], where marine-terminating glaciers, also called tidewater glaciers, play a central role in total glacier mass budget [16]. These glaciers were often believed to follow the tidewater glacier cycle, alternating between advance, rapid retreat, and

 doi:10.20944/preprints202604.0745.v1

retracted stability [20–22]. While retreat was usually considered independent from climate [21], recent observations in Alaska show widespread retreat, suggesting that climatic warming has reached a point where it overrides stabilizing phases [18,23]. Columbia Glacier is one of the most prominent examples, having retreated more than 20 km since 1980 and losing 50% of its mass [16,20,23].

Frontal ablation, including ice discharge, is largely driven by glacier velocity, which is connected to retreat and terminus instabilities [18,24]. Seasonal variability in subglacial drainage systems modulates flow, with peak velocities typically occurring in spring and early summer [24,25]. Submarine melt, influenced by ocean temperature, can account for up to half of the incoming ice discharge at glacier termini during summer [26].

Few studies have examined the impact of frontal ablation on glacier mass balance, which limits accurate predictions of SLR [16,27]. Two regional estimates of decadal frontal ablation from marine-terminating glaciers exist for Alaska [16,19]. This study targets a more detailed temporal record by presenting a monthly series of ice discharge for all marine-terminating glaciers in Alaska between 2015 and 2021. Additionally, an estimate of frontal ablation is given by including manually derived glacier terminus area changes throughout the observation period. Lastly, the results are discussed by correlating them to climate variables from reanalysis data. The study also aims to develop a methodology which can be adopted for other regions by using openly accessible data.

2. Study Region

Alaska contains 27,000 glaciers, covering nearly 87,000 km² [10,28]. The glaciers are located in the Brooks Range, Alaska Range, and Coast Mountains, reaching elevations above 6,000 m [10,29]. Land-terminating glaciers account for 67%, lake-terminating glaciers for 20%, and marine-terminating glaciers for 13% of the total glacier area in Alaska [11].

Marine-terminating glaciers are only found in southern Alaska. Consequently, the study region extends along the Gulf of Alaska from northwest British Columbia and the Coast Mountains to the western Chugach Mountains [30], between 56 and 61°N (Figure 1). It includes the three Randolph Glacier Inventory (RGI) version 7.0 o2-subregions: Western Chugach (01-04), Saint Elias (01-05), and North Coast Ranges (01-06), all of which are part of the Alaska RGI region (01) [30]. Most of the RGI 7.0 glacier area did not change compared to the RGI version 6.0, making a comparison to previous studies easier [31].

In the studied subregions of Alaska, marine-terminating glaciers represent 17.7% of the glacier area [30]. These glaciers have undergone significant retreat since the Little Ice Age, when most had reached their maximum extent between the early 18th and late 19th centuries [10,16,32,33].

Marine-terminating glaciers are particularly important because of their strong contribution to mass loss and SLR. Mc Nabb et al. [16] analyzed 50 of such glaciers with a total area of ~12,000 km², showing that just four glaciers - Columbia, Hubbard, Yahtse, and LeConte - accounted for 65% of the total frontal ablation between 1985 and 2013. Their incomplete understanding, including the role of fjord geometry and ocean forcing, remains a challenge for accurately predicting future contributions to SLR [16,34].

Alaska's climate is characterized by strong spatial gradients in temperature and precipitation. The environment ranges from subpolar to polar zones, with tundra vegetation and widespread boreal forests [35]. Climatic variability is primarily governed by latitude, elevation, and ocean proximity, with maritime conditions along the Coast Mountains and more continental climates in the Alaska Range [10,36]. Precipitation varies strongly, from approximately 200 mm annually in the North to up to 8,000 mm in the southern Coast Mountains, which act as a barrier to Pacific air masses [11,37]. Large-scale atmospheric drivers include the Aleutian Low and the Pacific Decadal Oscillation (PDO), with positive PDO phases linked to warmer and wetter conditions [11,32]. Both long-term warming and increased precipitation have been observed in Alaska, accompanied by a shortening of the snow season and a longer persisting melt season [32,38,39].

 doi:10.20944/preprints202604.0745.v1

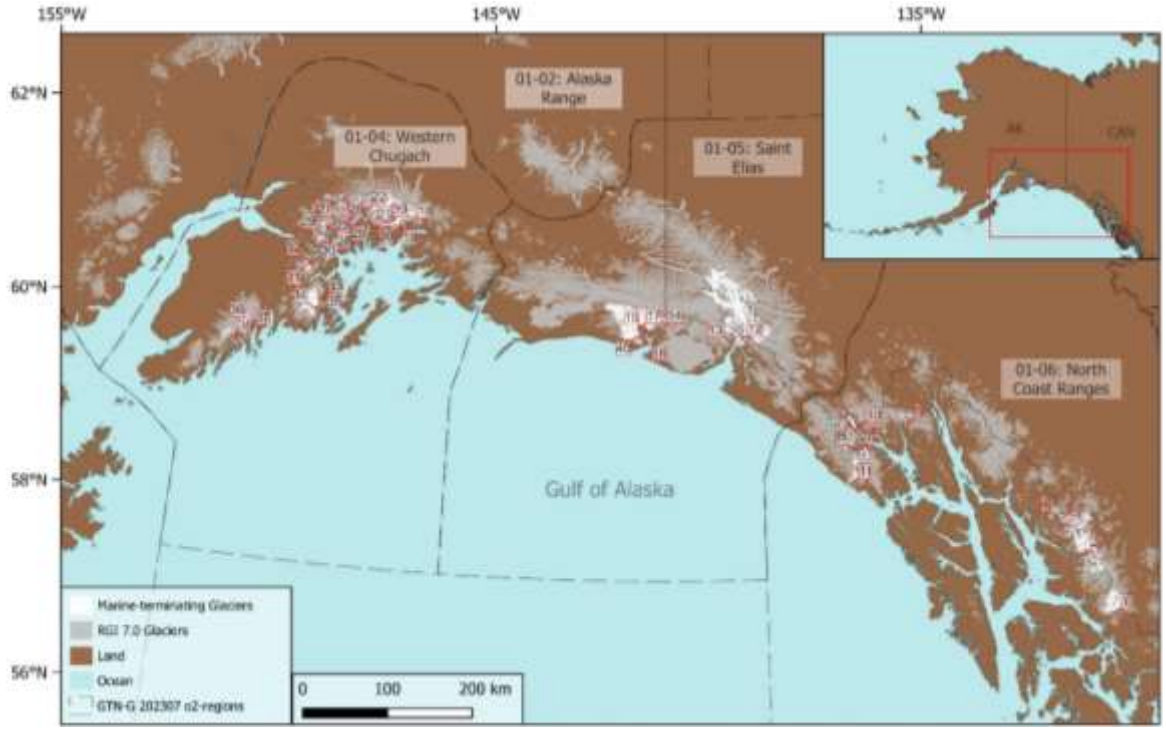

Figure 1. Overview of the study region in Alaska. Marine-terminating glaciers (white) and Randolph Glacier Inventory 7.0 [30] glaciers (lightgrey). Political boundaries (grey) and land areas (brown) are from GADM. RGI 7.0 subregions (dotted) are from the Global Terrestrial Network for Glaciers (GTN-G).

3. Materials and Methods

3.1. Ice Discharge Calculation

Ice discharge is defined as the mass or volumetric flux of ice through a vertical cross section called 'flux gate', which is perpendicular to the flow of ice [17]. Precise estimation of ice discharge from marine-terminating glaciers is important for quantifying their mass loss [40].

The volumetric ice discharge is calculated by multiplying ice velocity with the cross-sectional area (ice thickness), while integrating over a flux gate (see Figure 2) [28,40,41]. The formula after Rott et al. [42] was adapted to calculate the ice discharge rate ($\dot{D}_{ice}$, in Gt a^{-1}):

$$\dot{D}_{ice} = \sum_{n=1}^{N} \rho w_n H_n u_n cos(\alpha_n) \quad (1)$$

where N is the total number of flux gate segments, ρ is the density of ice, w_n is the width of a flux gate segment at flux gate point n, H_n the ice thickness of the segment, u_n is the mean velocity of the vertical ice column and α_n is the angle between the velocity vector and the angle perpendicular to the flux gate for the respective segment. The surface velocity v is used to estimate u_n, which is assumed to represent 95% of the former – leading to the expression: $u_n = 0.95v$ [19,42].

The ice volume flux is converted into the final mass flux by assuming an ice density ρ of 917 kg m^{-3} [17]. Ice velocity and thickness are point sampled at 100 m intervals along the flux gate – defined as flux gate segments. Ice thickness from Millan et al. [12] was temporally corrected for each ice discharge calculation as ice thickness data was only available from a reference date in July 2021. Surface elevation change data (dh/dt) from Hugonnet et al. [43] is taken for temporal ice thickness correction. Surface velocity magnitudes and flow angles are taken from the Sentinel-1 glacier flow database RETREAT [44].

Angles where $\alpha_n > 90°$ are assumed to be poorly constrained measurements and are set to the flux gate segment's perpendicular angle with a velocity of 5 m a^{-1}. Such angles likely indicate noisy

 doi:10.20944/preprints202604.0745.v1

data or very slow flowing glacier segments. Final ice discharge values of the segments are linearly interpolated to fill gaps along each flux gate.

The dataset from Friedl et al. [44] consists of surface velocities and flow angles derived from Sentinel-1 Synthetic Aperture Radar (SAR) images by applying intensity offset tracking. The resulting monthly or annually averaged scene-pair velocity fields have a spatial resolution of 200 m with an uncertainty < 0.08 m d^{-1}. The angles are provided in degrees of displacement relative to true north. Monthly velocity magnitude and angle products are downloaded from the database between January 2015 and September 2021. Several months have poor coverage, especially during 2015 and 2016, while January 2021 is completely missing.

A recent glacier thickness dataset based on the shallow-ice approximation [45] is publicly available from Millan et al. [12]. The ice thickness dataset has a spatial resolution of 50 m with mean errors of 25 – 35% for ice thickness values >100 m [12].

The flux gates are defined after Rott et al. [42]. Flux gates are usually chosen close to the calving front to avoid a correction of surface mass balance for the area between the calving front and the gate [41]. They also need to be positioned perpendicular to the flow direction of ice which can be difficult for glacier systems with a complex geometry, e.g. multiple glacier branches [40]. The flux gates were positioned for the year 2020 with the help of Landsat-8 optical imagery and have a length of ~100 km for the entire study region. While positioning the flux gate, it is paid attention to the coverage of ice thickness and velocity data to minimise data gaps in the following ice discharge calculation. However, some minor gaps remained in the data (Figure 2). All files included in the ice discharge calculation were projected into the coordinate system EPSG:32607 - WGS 84.

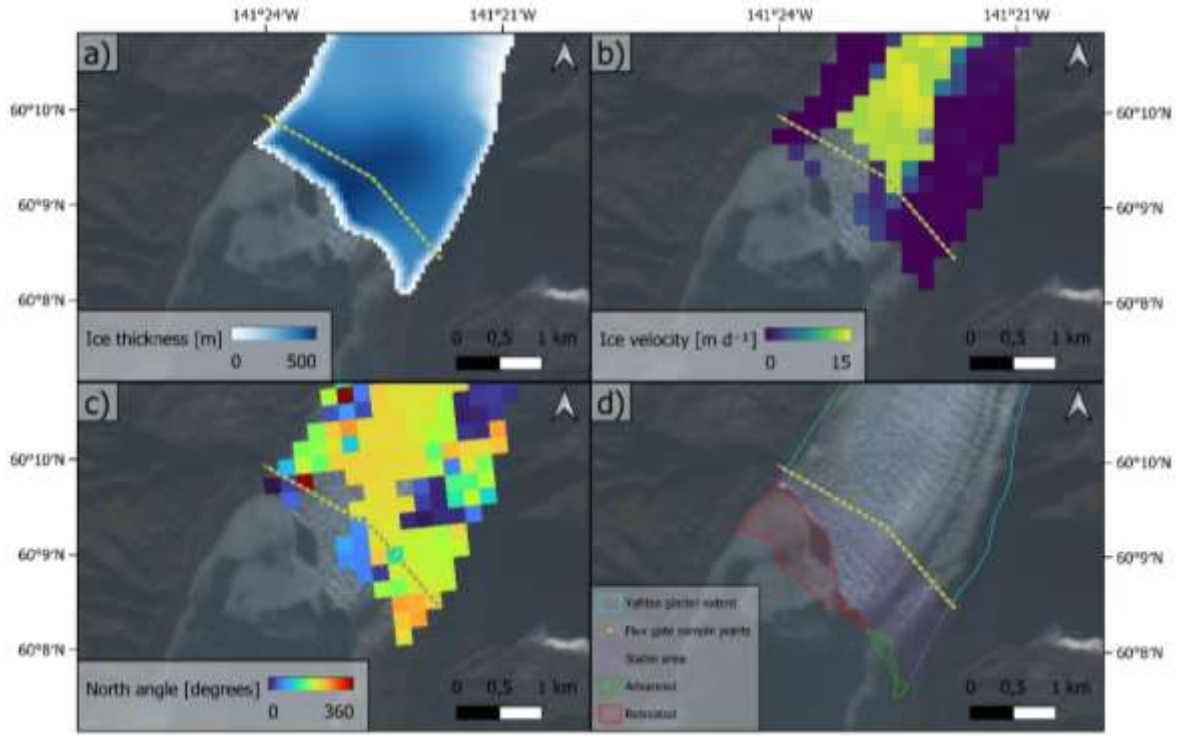

Figure 2. Input variables, exemplarily for Yahtse glacier. a) Ice thickness in meters [12], b) ice velocity in meters per day [12] and c) north angles in degrees [12] from 2021-07 and d) glacier terminus with flux gate and sample points along the flux gate (yellow), Yahtse glacier Randolph Glacier Inventory 7.0 outline [30] (light-blue), stable area S_f (purple), advanced area (green) and retreated area (red). Background is from Landsat 8 2020-10-10 [49]. .

The ice discharge is calculated for all distinct glacier termini contacting the ocean in 2020 – therefore a glacier may have multiple flux gates. In total, 45 flux gates are drawn for 40 glaciers. Two flux gates were drawn for Tsaa glacier and six for Columbia glacier with two for the eastern branch

 doi:10.20944/preprints202604.0745.v1

and four for the western branch. Columbia glacier consisted of two branches since 2010 [24], which split up further before 2020. To stay consistent with naming, the four western flux gates are summarized as First Branch Columbia glacier and the two eastern flux gates as Columbia glacier, after RGI 7.0 [30].

Ice discharge is estimated as previously described by using a flux gate near but not directly on the glacier terminus [42]. The climatic mass balance (CMB) – accumulation or ablation processes – on the area between flux gate and terminus is not considered within ice discharge and terminus mass change [17,46]. By neglecting this contribution, frontal ablation might be overestimated by up to 19% [16,41]. Concerning ice discharge and terminus mass change, the overestimation might be up to 20% and 9%, respectively, as reported by Kochtitzky et al. [19]. The CMB, $\dot{B}_{clim}$, is used to correct the terminus mass change ($\dot{M}_{term}$) and the ice discharge ($\dot{D}_{ice}$). $\dot{B}_{clim}$ comprises processes such as snow accumulation and melt at the surface, refreezing of melt or rain at the surface and melt or refreezing below the surface [19]. The climatic mass balance rate $\dot{B}_{clim}$ can be estimated by only including surface mass balance, while the minor contribution from internal and basal mass balances can be neglected [16,19,41,47]. $\dot{B}_{clim}$ is approximated here by calculating the mass change due to elevation change with dh/dt data from Hugonnet et al. [15]. This estimate already contains mass change due to surface mass balance [47] and potential dynamic thinning is neglected. The mean elevation change from 2015 to 2020 was -4.14 ± 5.92 m a^{-1} on the area uninvolved in terminus retreat or advance (S_f) below the flux gates [15]. Other studies [16,47] account for the surface mass balance by taking a fixed value of -10 m w.e. a^{-1} (m.w.e. = meters water equivalent) which corresponds to the highest value found on Columbia Glacier by Rasmussen et al. [48]. $\dot{B}_{clim}$ is estimated for all areas downstream of the fluxgate (including unchanged area, lost and gained area, see Figure 1d), by calculating the mass change from the mean elevation change for each glacier and converting those values into the mean specific climatic mass balance rate, given in kg m^{-2} a^{-1}. The corrected ice discharge ($\dot{D}_{ice_{cor}}$) was then calculated after Kochtitzky et al. [19]:

$$\dot{D}_{ice_{cor}} = \dot{D}_{ice} + \left(S_f * \dot{B}_{clim}\right) \quad (2)$$

with the ice discharge rate $\dot{D}_{ice}$ (Gt a^{-1}), the area below the fluxgate which did not retreat or advance (S_f, in m^2) and the mean specific climatic mass balance rate named $\dot{B}_{clim}$ (kg m^{-2} a^{-1}).

Terminus mass change was estimated following Kochtitzky et al. [19] by manually digitizing glacier fronts from Landsat 8 images for 2015 and 2020 [49]. The area lost or gained was combined with mean ice thickness and $\dot{B}_{clim}$ to compute mass loss rates [16,19,47]. Terminus mass loss is indicated by a negative sign and terminus mass gain by a positive sign according to Kochtitzky et al. [19]. Frontal ablation was then calculated as the sum of ice discharge and terminus mass change after Cogley et al. [17] and Kochtitzky et al. [19].

3.2. Uncertainty

Ice discharge uncertainty is estimated by computing velocity and angle errors from Friedl et al. [44] ice velocities and angles. Ice thickness errors are provided in the dataset from Millan et al. [12]. From the ice discharge term (Eq. 1) similar to Kochtitzky et al. [19] follows:

$$\sigma^2{}_{\dot{D}_{ice}} = \rho \sum_n \left(\left(\frac{\partial_{\dot{D}_{ice}}}{\partial_{H_n}} \sigma_{H_n} \right)^2 + \left(\frac{\partial_{\dot{D}_{ice}}}{\partial_{u_n}} \sigma_{u_n} \right)^2 + \left(\frac{\partial_{\dot{D}_{ice}}}{\partial_{\alpha_n}} \sigma_{\alpha_n} \right)^2 \right) \quad (3)$$

and for the corrected ice discharge $\sigma_{\dot{D}_{ice_{cor}}}$ with $\sigma_{\dot{B}_{clim}}$:

$$\sigma^2{}_{\dot{D}_{ice_{cor}}} = \left(\sigma_{\dot{D}_{ice}}\right)^2 + \left(S_f * \sigma_{\dot{B}_{clim}}\right)^2 + \left(\sigma_{S_f} * \dot{B}_{clim}\right)^2 \quad (4)$$

where σ_{H_n} and σ_{u_n} are the uncertainties for ice thickness and velocity at flux gate point n, respectively. σ_{α_n} is the angle uncertainty. $\sigma_{\dot{B}_{clim}}$ is the uncertainty of the mean specific climatic mass balance rate which is calculated by taking the elevation change error from Hugonnet et al. [15]. σ_{S_f} is the uncertainty of gained or lost area below the flux gate, determined from its perimeter multiplied by the width of one pixel, which is 30 m for Landsat [19,47,50].

 doi:10.20944/preprints202604.0745.v1

Millan et al. [12] report an uncertainty of 30% for their modelled glacier thickness. Uncertainties are primarily related to the surface slope, ice velocity, and for several glaciers exhibiting surge type behaviour [12]. The study by Millan et al. [12] identified four surging glaciers in Alaska from 2015 to 2019 for which they increased their uncertainty estimate up to 75%. However, no further evaluation of potentially surging glaciers during the study period was carried out.

The uncertainty of ice velocity can be estimated by calculating ice velocity over ice free land areas, which are assumed to be motionless, or by in-situ measurements [51,52]. Since the latter was not available, the median ice velocity for all pixels classified as land was taken as an uncertainty value. Sánchez-Gámez and Navarro [41] concluded that the angle uncertainty can be neglected due to a low contribution to the ice discharge uncertainty. However, here, the angle uncertainty σ_{α_n} was estimated with the formula after Mouginot et al. [51]:

$$\sigma_{\alpha_n} = \frac{\sigma_{u_n}}{2 * u_n} \quad (5)$$

with the uncertainty in velocity σ_{u_n} and the velocity u_n.

3.3. Atmospheric Data

Atmospheric data from the fifth generation of European ReAnalysis (ERA5) is used to investigate the glacier-climate relationship for marine-terminating glaciers in Alaska. ERA5 is produced by the European Centre for Medium-Range Weather Forecasts (ECMWF), which is embedded within the Copernicus Climate Change Service (C3S) from the European Commission [53].

Monthly averaged data from the ERA5-Land dataset is used from the Copernicus Climate Data Store [53]. The ERA5-Land monthly averaged dataset contains air temperature 2 m above ground (K), snowfall (m w.e.) and total precipitation (m), which were downloaded for the study period spanning from 2015-01-01 to 2021-09-01 [54]. The data is extracted for each glacier location at the flux gate and mean values from all glaciers are calculated. The air temperature above 2 m (further referred to as surface temperature) is converted into degrees Celsius. Correlation analysis was carried out using Spearman's rank correlation test because the data is not normally distributed [55]. Trends are analysed first by decomposing the timeseries data with Seasonal Decomposition of Time Series by Loess (STL) after Cleveland et al. [56], before applying a linear regression [55].

3.4. Ocean Temperature Data

The Global Oceanic and Sea-Ice Reanalysis (GLORYS12) dataset is used for further analysis regarding ocean-glacier interaction, as it includes a three dimensional dataset of ocean temperature and is available at 1/12 degrees horizontal resolution [57]. GLORYS12 covers 50 vertical levels from 1993 onward and is part of the Copernicus Marine Environment Monitoring Service (CMEMS) [58]. The dataset was produced by using in situ and satellite observations, numerical modelling and data assimilation [57].

The GLORYS12V1 monthly product was downloaded from the Marine Data Store [58] for the period 2015-01-01 to 2021-06-01. The variable sea water potential temperature (°C), from now on referred to as ocean temperature, is used for further analysis. As coverage was not always available close to the glacier termini, a buffer of 50 km distance was placed around the flux gates and the mean of those pixels is taken from the GLORYS12 data for each glacier. For that reason, some glaciers are sampled with similar or identical ocean temperature samples because they are located in the same fjord. Some glaciers have to be sampled further away due to poor coverage. For Columbia glacier for example, coverage starts 16 km south of its terminus.

Due to differing spacing between each depth level, the depth weighted mean is calculated from the ocean temperature data. A maximum of 32 depth levels, equal to a depth from 0.49 to 541.09 m is chosen, accounting for typical fjord depth and ice thickness. The mean thickness at the flux gates was 248 ± 72 m [12]. The mean fjord depth at all glacier termini is 241 m, which was retrieved from the

 doi:10.20944/preprints202604.0745.v1

southern Alaska coastal relief model [59]. Finally, a correlation analysis was performed as described in Section *3.3*.

3.5. Seasonal Patterns

Seasonal effects have strong controls on submarine melt and subglacial discharge, and thus glacier velocities [26,60]. Marine-terminating glaciers show different seasonal velocity patterns which can be determined either by terminus position change or meltwater [61].

Therefore, seasonal variability is analysed according to Moon et al. [61] and glaciers are assigned into three categories of behaviour. Type 1 behaviour is characterized by a glacier velocity speedup between late spring and early summer. Velocity remains high until it decreases in late winter or early spring. For Type 2, velocity strongly increases during early summer and decreases during mid-summer. Winter velocities can be higher than during spring and fall but mostly remain lower than during summer. Type 3 is distinguished by a late summer minimum. Over the winter, velocity steadily increases before it begins slowing down during mid-summer [61].

For the seasonal characterization, the mean glacier velocity from Friedl et al. [44] is taken at the flux gates and linearly detrended. The mean velocity is computed for each month and glacier. This seasonal velocity variability is then used to manually identify the type of behaviour for each glacier after Moon et al. [61].

4. Results

Table 1. Results for each glacier between 2015 and 2021. For Glacier location see Figure 1.

Terminus Mass Change [Gt a^{-1}]	Ice Discharge [Gt a^{-1}]	Frontal Ablation [Gt a^{-1}]	Area Change [km^2]	Glacier Name	ID-Number
-0.0044 ± 0.0002	0.03 ± 0.05	0.04 ± 0.05	-0.09 ± 0.06	LeConte Glacier	01
-0.1626 ± 0.0055	0.54 ± 0.19	0.70 ± 0.19	-2.47 ± 0.24	Dawes Glacier	02
-0.0515 ± 0.0038	0.45 ± 0.17	0.50 ± 0.17	-0.98 ± 0.13	South Sawyer Glacier	03
-0.0009 ± 0.0003	0.01 ± 0.09	0.01 ± 0.09	-0.02 ± 0.03	Sawyer Glacier	04
-0.0433 ± 0.0031	0.06 ± 0.06	0.10 ± 0.06	-1.27 ± 0.15	McBride Glacier	05
-0.0158 ± 0.0010	0.02 ± 0.02	0.03 ± 0.02	-0.55 ± 0.14	Lamplugh Glacier	06
-0.0009 ± 0.0001	0.004 ± 0.008	0.01 ± 0.01	-0.06 ± 0.03	Gilman Glacier	07
-0.0020 ± 0.0002	0.21 ± 0.08	0.21 ± 0.08	-0.19 ± 0.09	Johns Hopkins Glacier	08
-0.0091 ± 0.0010	0.13 ± 0.07	0.14 ± 0.07	-0.42 ± 0.13	Margerie Glacier	09
-0.0004 ± 0.0001	0.02 ± 0.11	0.02 ± 0.11	-0.04 ± 0.09	Grand Pacific Glacier	10
0.00 ± 0.03	0.04 ± 0.12	0.04 ± 0.13	0.00 ± 0.10	La Perouse Glacier	11
-0.0274 ± 0.0023	4.49 ± 1.30	4.51 ± 1.30	-0.77 ± 0.22	Hubbard Glacier	12

 doi:10.20944/preprints202604.0745.v1

0.012 ± 0.001	0.012 ± 0.055	0.000 ± 0.055	0.90 ± 0.17	Turner Glacier*	13
0.00002 ± 0.00012	0.02 ± 0.03	0.02 ± 0.03	0.15 ± 0.09	Tyndall Glacier	14
-0.0167 ± 0.0007	0.76 ± 0.30	0.78 ± 0.30	-0.69 ± 0.08	Yahtse Glacier	15
-0.00001 ± 0.00003	0.01 ± 0.04	0.01 ± 0.04	-0.03 ± 0.02	Grotto Glacier	16
-0.0005 ± 0.0009	0.06 ± 0.08	0.06 ± 0.08	-0.34 ± 0.08	Guyot Glacier	17
-0.0003 ± 0.0001	0.01 ± 0.06	0.01 ± 0.06	-0.03 ± 0.02	Shoup Glacier	18
-0.7333 ± 0.0191	2.70 ± 0.94	3.43 ± 0.94	-14.30 ± 0.72	Columbia Glacier	19
0.00016 ± 0.00004	0.17 ± 0.08	0.17 ± 0.08	0.03 ± 0.04	Meares Glacier	20
-0.0058 ± 0.0005	0.11 ± 0.04	0.11 ± 0.04	-0.19 ± 0.07	Yale Glacier	21
0.0001 ± 0.0002	0.48 ± 0.22	0.48 ± 0.22	0.15 ± 0.11	Harvard Glacier	22
-0.0014 ± 0.0004	0.002 ± 0.007	0.003 ± 0.007	-0.12 ± 0.06	Smith Glacier	23
0.00001 ± 0.00002	0.01 ± 0.02	0.01 ± 0.02	0.0005 ± 0.0094	Bryn Mawr Glacier	24
-0.0026 ± 0.0008	0.14 ± 0.08	0.14 ± 0.08	-0.12 ± 0.06	Barry Glacier	25
0.000003 ± 0.000019	0.003 ± 0.014	0.003 ± 0.014	0.003 ± 0.012	Cascade Glacier	26
-0.00004 ± 0.00005	0.01 ± 0.02	0.01 ± 0.02	-0.01 ± 0.02	Coxe Glacier	27
-0.0252 ± 0.0027	0.16 ± 0.12	0.19 ± 0.12	-0.80 ± 0.12	Surprise Glacier	28
-0.0013 ± 0.0002	0.03 ± 0.13	0.03 ± 0.13	-0.12 ± 0.12	Harriman Glacier	29
-0.00008 ± 0.00004	0.05 ± 0.04	0.05 ± 0.04	-0.01 ± 0.02	Beloit Glacier	30
-0.000001 ± 0.000010	0.03 ± 0.03	0.03 ± 0.03	-0.003 ± 0.020	Blackstone Glacier	31
-0.00004 ± 0.00005	0.002 ± 0.009	0.002 ± 0.009	-0.01 ± 0.02	Northland Glacier	32
-0.0203 ± 0.0025	0.56 ± 0.21	0.58 ± 0.21	-0.70 ± 0.21	Chenega Glacier	33
-0.0007 ± 0.0003	0.04 ± 0.03	0.04 ± 0.03	-0.04 ± 0.05	Tiger Glacier	34
-0.0151 ± 0.0010	0.03 ± 0.05	0.04 ± 0.05	-0.51 ± 0.11	Bainbridge Glacier	35
-0.0037 ± 0.0008	0.07 ± 0.08	0.08 ± 0.08	-0.24 ± 0.11	Aialik Glacier	36
0.0025 ± 0.0004	0.05 ± 0.03	0.05 ± 0.03	0.22 ± 0.06	Holgate Glacier	37
-0.0012 ± 0.0005	0.03 ± 0.08	0.03 ± 0.08	-0.11 ± 0.04	McCarty Glacier	38
-0.1681 ± 0.0186	0.23 ± 0.18	0.40 ± 0.18	-5.31 ± 0.36	First Branch Columbia Glacier	39
-0.0026 ± 0.0006	0.04±0.10	0.04 ± 0.10	-0.17 ± 0.09	Tsaa Glacier	40
-1.30 ± 0.07	**11.81±5.35**	**13.11 ± 5.35**	**-29.24 ± 4.19**	**Total**	

* Turner glacier had higher correction values than ice discharge, therefore, uncorrected frontal ablation and ice discharge values are shown instead of the CMB corrected values.

4.1. Ice Discharge

 doi:10.20944/preprints202604.0745.v1

For all 40 glaciers within the study region, the average ice discharge from January 2015 to September 2021 was 11.81 ± 5.35 Gt a^{-1}. Per glacier, the yearly ice discharge was 0.05 ± 0.07 Gt a^{-1} on average (median: 0.04 ± 0.07 Gt a^{-1}) and with a standard deviation of 0.81 ± 0.24 Gt a^{-1}. The glaciers which had the highest contributions were Hubbard glacier (4.49 ± 1.30 Gt a^{-1}), Columbia glacier (2.93 ± 1.12 Gt a^{-1}; both branches together) and Yahtse glacier (0.76 ± 0.30 Gt a^{-1}). These three glaciers together represented ~70% of the entire ice discharge (Table 1).

4.2. Terminus Mass Loss

The total manually derived area change at the glacier termini from Juli 2015 to October 2020 is -29.24 ± 4.19 km², indicating an overall area loss (Table 1). La Perouse glacier did not change during the study period (Figure 3a), 7 glaciers gained area (Turner, Tyndall, Meares, Harvard, Bryn Mawr, Cascade and Holgate glacier), and 32 of the glaciers lost area. The area gained on the terminus accounts for 2.07 ± 1.02 km² while the lost area contributes -31.31 ± 4.23 km². It is clearly visible (Figure 3 a) that both branches of Columbia glacier contribute the most by losing 19.62 ± 1.08 km², explaining two thirds of the total area change. The mean area change is -0.73 ± 0.10 km² (median change: -0.11 ± 0.08 km²) with a standard deviation of 2.37 ± 0.12 km².

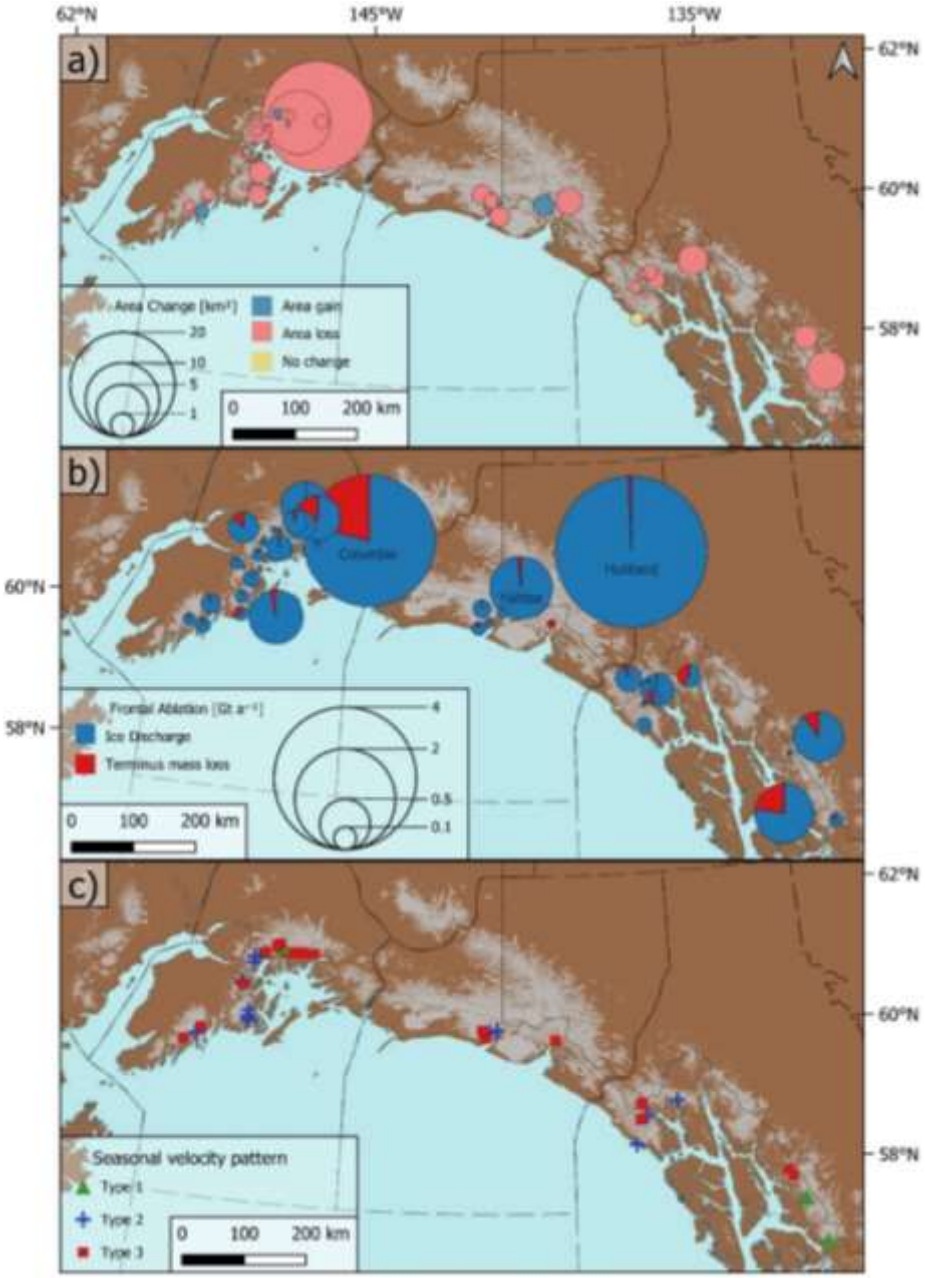

 doi:10.20944/preprints202604.0745.v1

Figure 3. a) Glacier area changes in km² from 2015 to 2020. Blue denotes area gain and red area loss. One glacier area did not change (La Perouse) indicated by yellow. b) Frontal ablation as the sum of ice discharge and terminus mass loss (Gt a^{-1}) between 2015 and 2021. c) Geographical distribution of Type 1 (green triangle), Type 2 (blue cross) and Type 3 (red square) classified after Moon et al. [61]. .

The net terminus mass loss during the study period was 1.30 ± 0.07 Gt a^{-1}. Some glaciers advanced (Turner, Tyndall, Meares, Harvard, Bryn Mawr, Cascade and Holgate glacier), and one glacier was stable (La Perouse). However, 32 of 40 glaciers (80%) retreated at the terminus from 2015 to 2021. The mass loss of 1.33 ± 0.07 Gt a^{-1} exceeded the mass gain from advance of 0.028 ± 0.003 Gt a^{-1} (Table 1).

The largest contributors were Columbia glacier with -0.73 ± 0.02 Gt a^{-1}, First Branch Columbia glacier with -0.17 ± 0.02 Gt a^{-1} and Dawes glacier with -0.163 ± 0.006 Gt a^{-1}. The mean terminus mass change was -0.033 ± 0.002 Gt a^{-1} (median: -0.0012 ± 0.0004 Gt a^{-1}) with a standard deviation of 0.118 ± 0.004 Gt a^{-1}.

4.3. Frontal Ablation

The total frontal ablation from 2015 to 2021 was 13.11 ± 5.35 Gt a^{-1}. The mean frontal ablation was 0.33 ± 0.13 Gt a^{-1} (median: 0.04 ± 0.07 Gt a^{-1}). On average, ice discharge explains ~89% of the entire frontal ablation. For several glaciers, and for example Turner glacier, terminus mass loss contributed more to frontal ablation than ice discharge. The results for all glaciers are summarized in Table 1.

Hubbard and Columbia glacier are the largest contributors to frontal ablation. While ice discharge made up 99.6% of Hubbard glacier's frontal ablation, it accounted for 78.7% of Columbia glacier's and 57.5% of the First Branch Columbia glacier's frontal ablation. Turner glacier received a negative ice discharge value because the CMB correction value (Eq. 2) was higher than the uncorrected ice discharge, which seems to be unrealistic. This would also result in a negative frontal ablation value. Consequently, the uncorrected ice discharge value for Turner glacier of 0.012 ± 0.055 Gt a^{-1}. is used for further analysis. Turner glacier's terminus, however, advanced and gained 0.012 ± 0.001 Gt a^{-1} which means that the frontal ablation results to zero (Table 1). For area change, ice discharge and terminus mass loss, see Figure 3.

4.4. Seasonality

Four glaciers (8.9%) were assigned to Type 1 behaviour, thirteen (28.9%) were classified as Type 2 and twenty-seven (60%) as Type 3 (Figure 3c). Turner glacier was not clearly distinguishable as velocity decreases from January onwards reaching a low in July (Figure 4d). Afterwards, velocity shortly peaks in September and decreases again in October. Glacier velocity data was analysed for each flux gate, with the multiple flux gates of Tsaa and Columbia glaciers considered separately. For both Tsaa gates and all Columbia gates, Type 3 behaviour was observed. Overall, Type 3 was the dominant category representing ~60% of all glaciers.

All types are scattered across the study region, and therefore no clear geographical pattern is visible (Figure 3c). Dawes glacier for example (Figure 4a), located in the North Coast Ranges, was assigned to Type 1 as it shows a late winter/spring velocity deceleration followed by a late spring/early summer acceleration. Chenega glacier (Figure 4b) is characterized by an early summer speedup and mid-summer slow-down and was for that reason classified as Type 2. Winter velocity is elevated but it remains lower than the summer maximum. Type 3 behaviour is observed e.g. for Harvard glacier (Figure 4c), whose seasonal velocity is governed by a mid-summer slowdown which leads to a pronounced late summer minimum. After that, velocity steadily increases again.

 doi:10.20944/preprints202604.0745.v1

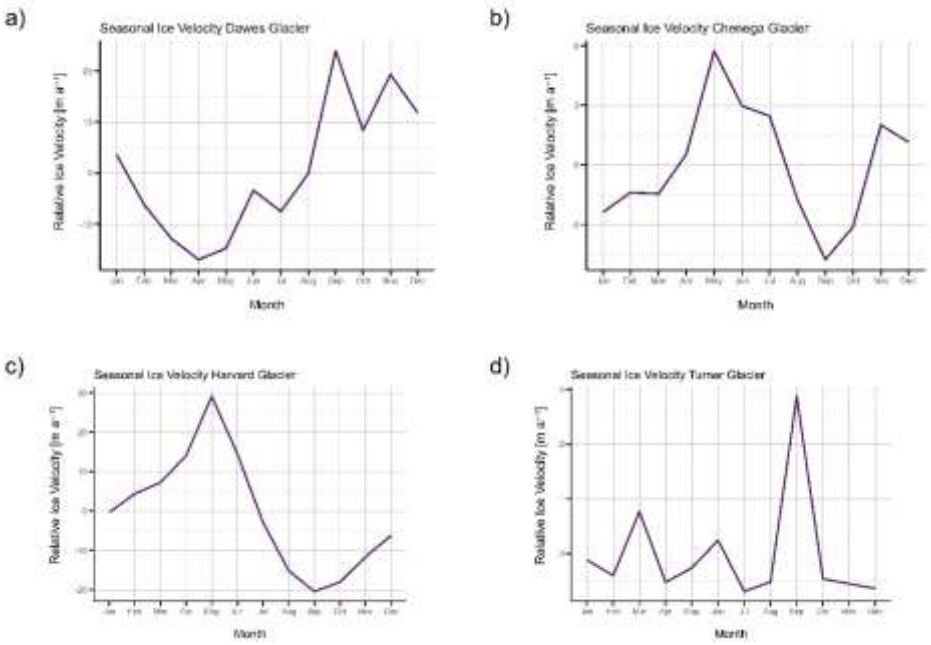

Figure 4. Seasonal velocity patterns with examples for a) Type 1, b) Type 2 and c) Type 3 behaviour after Moon et al. [61]. Turner glacier d) was not assigned to any type. .

4.5. Climate-Glacier Relationship

Ice discharge and surface temperature showed a moderate negative Spearman correlation of $\varrho = -0.37$ ($p < 0.001$). The relationship between precipitation and ice discharge was not significant (Spearman $\varrho = -0.20$, $p = 0.07$). Rainfall was moderately negatively correlated with ice discharge, with $\varrho = -0.54$ ($p < 0.001$). Snowfall, on the other hand, showed a weak positive correlation with ice discharge ($\varrho = 0.26$, $p < 0.05$), compare Figure 5.

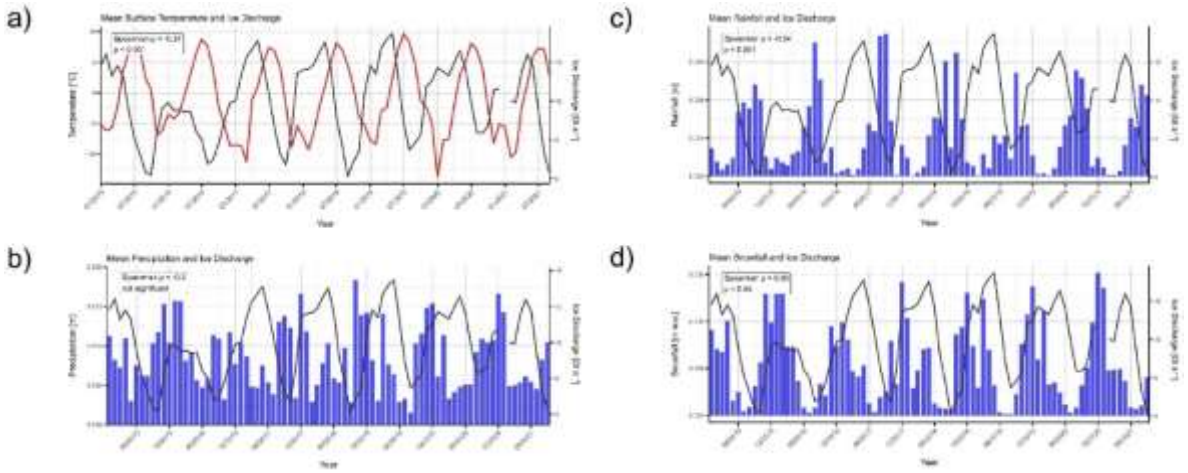

Figure 5. a) Mean surface temperature in degrees Celsius (red line), b) mean precipitation (blue) in meters, c) mean rainfall (blue) in meters and d) mean snowfall (blue) in meters water equivalent (m w.e.) d) of all glaciers with ice discharge (black line) in Gigatons per year (Gt a^{-1}) are depicted. The spearman correlation coefficient ϱ and the significance p are shown for each variable. .

The strongest relationship was found with ocean temperature (Figure 6). Weighted mean ocean temperature was strongly and negatively correlated with average ice discharge, with $\varrho = -0.72$ ($p < 0.001$). Hubbard and Columbia glacier exhibited strong negative correlations of -0.62 ($p < 0.001$) and

 doi:10.20944/preprints202604.0745.v1

-0.65 ($p < 0.001$). Ocean temperature at Yahtse glacier conversely showed a low positive correlation with ice discharge (Spearman $\varrho = 0.23$, $p < 0.05$). This relationship was most prominent during September. Compared to 2015, ocean temperatures for 2016, 2019 and 2020 are warmer. However, during 2017 and 2018, temperatures dropped, especially below 50 m depth. Overall, mean ocean temperatures increased by 0.16 °C (0.002 °C per month) from January 2015 to June 2021.

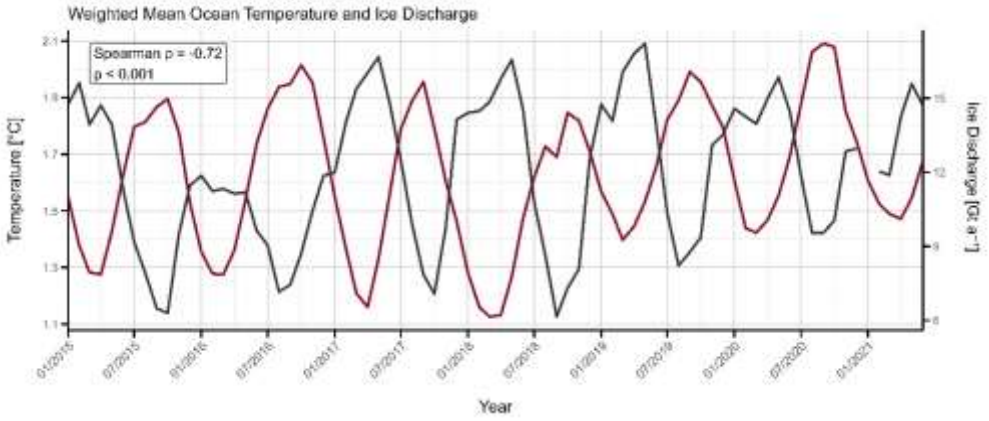

Figure 6. Weighted mean ocean temperature (red) and ice discharge (black) with spearman correlation coefficient ϱ and significance level p indicating high significance. .

In contrast to ocean temperature, all other variables showed decreasing trends (Figure 8). Simultaneously, the PDO switched from positive to negative. Surface temperature decreased by 1.26 °C (0.02 °C per month), total precipitation by 1.1 mm (0.014 mm per month), snowfall by 0.000550 m w.e. (0.000007 m w.e. per month) and rainfall by 0.5945 mm (0.0073 mm per month). All trends, PDO excluded, were found to be highly significant ($p < 0.001$).

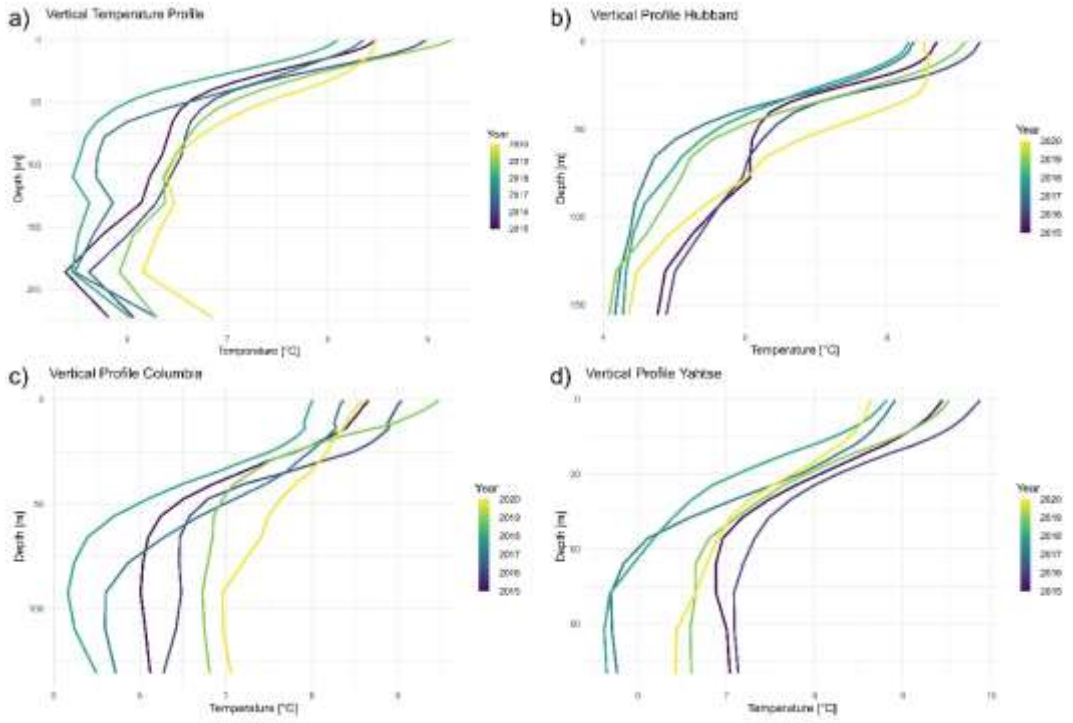

Figure 7. Vertical profiles of ocean temperatures between 2015 and 2020 a) for all glaciers averaged, b) Hubbard glacier, c) Columbia glacier and d) Yahtse glacier. .

 doi:10.20944/preprints202604.0745.v1

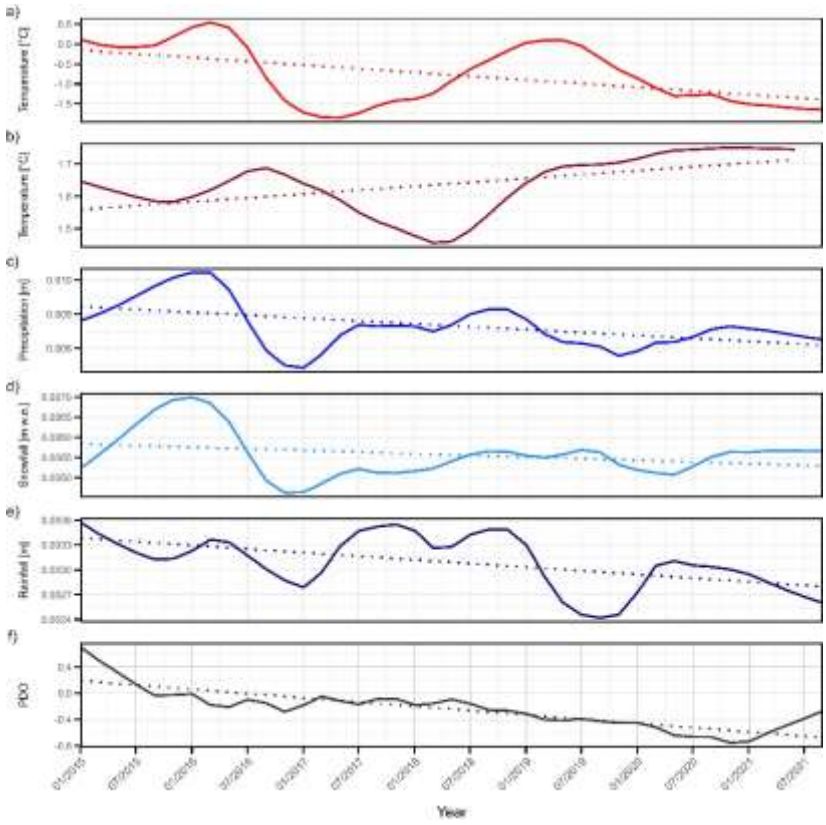

Figure 8. Trends of climate variables after seasonal decomposition with STL (line) and after linear regression (dotted) for surface temperature a) in red, ocean temperature b) in dark-red, precipitation c) in blue, snowfall d) in light blue, rainfall e) in dark blue and Pacific Decadal Oscillation (PDO) f) in black. .

5. Discussion

5.1. Comparison to Other Studies

Several studies have quantified frontal ablation of Alaskan glaciers over different periods, glacier types, and using varying methodological approaches [16,19,47]. Although these studies broadly agree that frontal ablation represents a major component of glacier mass loss, substantial differences exist in reported rates of frontal ablation and ice discharge. These discrepancies can largely be attributed to differences in study period, glacier type (marine- vs. lake-terminating), ice thickness and velocity data, treatment of CMB between flux gate and terminus, and dominant glacier contributions.

McNabb et al. [16] reported a mean frontal ablation rate of 15.11 ± 3.63 Gt a^{-1} and a total ice discharge of 15.4 Gt a^{-1} for the period 1985-2013, compared to 13.11 ± 5.35 Gt a^{-1} of frontal ablation and a mean ice discharge of 11.81 ± 5.35 Gt a^{-1} found here for the period 2015–2021. The study [16] investigated frontal ablation of 27 marine-terminating glaciers in Alaska, representing 96% of the total marine-terminating glacier area. Frontal ablation was computed by taking the sum of calving and submarine melt at the terminus while using a flux gate approach. Thickness variations were accounted for, while surface mass balance between the flux gate and terminus was approximated using a CMB of −10 m w.e. a^{-1} for all glaciers, corresponding to the maximum value observed at Columbia Glacier. This assumption is considerably more negative than the average CMB of −3.72 ± 5.33 m w.e. a^{-1} estimated for the same area in this study, and likely contributes to higher frontal ablation estimates for McNabb et al. Differences are further influenced by the study period, as McNabb et al. include years of particularly rapid retreat, especially at Columbia Glacier, which alone accounted for ~25% of total frontal ablation.

 doi:10.20944/preprints202604.0745.v1

Kochtitzky et al. [19] estimated frontal ablation and ice discharge of Northern Hemisphere marine-terminating glaciers from 2000 to 2010 and 2010 to 2020, including 42 glaciers in Alaska. For Alaska, frontal ablation rates decreased from 11.59 ± 0.39 Gt a^{-1} during 2000–2010 to 10.68 ± 0.33 Gt a^{-1} during 2010–2020, while ice discharge declined from 11.49 ± 0.35 Gt a^{-1} to 9.79 ± 0.18 Gt a^{-1} over the same periods. In contrast, terminus mass loss increased nearly tenfold. Compared to Kochtitzky et al., this study finds higher frontal ablation, ice discharge, and terminus mass loss for 2015–2021, which may reflect both methodological differences (e.g. thickness assumptions and velocity datasets) and differences in the observation periods. Nevertheless, both studies consistently show that frontal ablation is dominated by ice discharge (≈89–92%) and that a small subset of glaciers contribute disproportionately to total mass loss. Frontal ablation was defined consistently in Kochtitzky et al. and in this study as the sum of ice discharge and terminus mass change. Ice velocity data was mainly taken from annual displacement mosaics generated from Landsat of the Inter-mission Time Series of Land Ice Velocity and Elevation (ITS_LIVE). The study [19] used directly measured thickness data from the Glacier Thickness Database (GlaThiDa) 3.0.3 and accounted for thickness change during the study period by incorporating elevation change data from Hugonnet et al. [15]. Where no observations were available, they incorporated modelled ice thickness from Millan et al. [12]. Kochtitzky et al. [19] report that the modelled ice thickness was on average 135 m higher than observations on the fluxgate. Unlike McNabb et al. [16], they explicitly modelled the CMB between the flux gate and terminus rather than applying a constant value. Similar to this study, glacier terminus positions were mapped manually, primarily by using optical imagery (Landsat or ASTER) to calculate mass change due to terminus retreat or advance.

Caldwell et al. [47] focused on 55 lake-terminating glaciers in Alaska from 2009 to 2018 using a flux-gate approach like McNabb et al. [16]. The authors reported a total frontal ablation of 6.1 Gt a^{-1} for all lake-terminating glaciers combined, with a median frontal ablation rate of 0.04 Gt a^{-1}, which closely matches the median value found in this study (0.04 ± 0.07 Gt a^{-1}). In contrast to marine-terminating glaciers, ice discharge values and total frontal ablation were substantially lower. Caldwell et al. [47] show that nearly all lake-terminating glaciers retreated over recent decades, with higher mean retreat rates than marine-terminating glaciers yet lost substantially less mass overall. This contrast highlights the importance of the terminus environment: marine-terminating glaciers experience enhanced mass loss due to calving dynamics and submarine melt, even if retreat rates are lower on average. The dominance of individual glaciers, such as Columbia Glacier, also strongly influences mean retreat and mass loss statistics across all studies. Caldwell et al. [47] used ice thickness and velocity data from Millan et al. [12]. CMB between flux gate and terminus was approximated using a constant value of −10 m w.e. a^{-1} as in the study of McNabb et al. [16]. Terminus retreat was also determined by manually delineating glacier terminus positions between 1984 and 2021 from annual Landsat imagery [47].

5.2. Drivers

Glacier retreat is initiated if there is an imbalance between ice discharge and terminus mass loss [46]. Caldwell et al. [47] define two types of frontal ablation. The first one is active frontal ablation, where the incoming ice discharge is higher than the terminus mass loss. The other type is passive frontal ablation, which is characterized by low ice discharge rates but high terminus mass loss. Both of these types can lead to high frontal ablation rates but active frontal ablation may let the whole glacier react to terminus conditions with positive feedbacks [47]. In this study, ice discharge was found to be the most important driver of mass loss (see Section 4), and therefore, active frontal ablation dominates. However, it remains unclear how far a comparison of lake- and marine terminating glaciers is suitable.

5.2.1. Glacier Velocity

Ice discharge greatly depends on ice velocity [46], which is seasonally controlled [24] and tends to be higher under maritime climatic conditions [34]. Typically, velocities of glaciers in Alaska reach

 doi:10.20944/preprints202604.0745.v1

their maximum somewhere around spring and their minimum during late summer or fall [16,24,62]. We found Type 3 (see Section 3.5. and 4.4.) behaviour for most of the glaciers (60%) in the study area. This velocity pattern has been described for glaciers in Alaska by previous studies [16,24,34,62–64].

However, some glaciers may show characteristics of more than one pattern, e.g. Chenega glacier. Moon et al. [61] suggest that melt plays an important role for the Type 1 behaviour, where meltwater increases the velocity from spring to summer. High velocities through late summer and fall, combined with the observation that this pattern occurred for a few glaciers and not continuous over the years, indicated that Type 1 behaviour mostly depends on the glacier terminus position [61]. From the four Type 1 glaciers, Dawes glacier retreated the most (compare Table 1), while the others (Barry, LeConte and Yale glacier) did not retreat considerably.

Type 2 glaciers are associated with increasing runoff which accelerates ice velocity during early summer [61]. Some glaciers accelerated earlier or decelerated during late summer/spring. It is unclear whether those glaciers should be classified as Type 3 as of Type 2. A comparison with runoff data might help to better understand the dynamics, but this was beyond the scope of this study. Nevertheless, Type 2 behaviour implies that most of those glaciers do not have or only possess a weak drainage system [61].

The Type 3 pattern indicates that there is a change from an inefficient to an efficient drainage system due to decreasing velocity when runoff is high [61]. A majority of glaciers show this pattern clearly (e.g., Harvard glacier, see Figure 4c), with a pronounced maximum during spring and a minimum that most often appears in September or October (late summer/early fall). Turner glacier, which was not assigned to any type, could arguably be considered a Type 1 glacier, because terminus mass change was comparably high.

Enderlin et al. [23] also stated that the subglacial drainage system has greater effects on glacier velocity than terminus retreat or advance. Therefore, meltwater induces changes in basal motion depending on the evolution of the drainage system [62]. This leads to an offset between ice discharge and temperature. While the drainage channels for meltwater have not developed yet, the increasing availability of meltwater raises the pressure below the glacier, which induces basal motion and leads to a speedup in ice velocity [64]. As soon as the system is developed, meltwater starts draining and pressure is released which slows down the glacier's velocity [62]. Drainage channels start to close at the beginning of winter, and hence velocity starts increasing because of remaining summer meltwater [24] and rainwater entering the drainage system [62]. The correlation of ocean temperature and ice discharge indicates that this relationship is highly significant (Figure 6).

Glacier surges, defined as periodical changes in flow with exceptionally high velocities [18,34], can bias mass loss estimates and lead to higher frontal ablation rates [15,19]. The RGI 7.0 [30] suggests that only La Perouse glacier is known to surge in the study region. La Perouse glacier had very low mean velocities at the flux gate of 5.5 ± 1.5 m a^{-1} and did not advance or retreat. This indicates that La Perouse glacier was possibly in a quiescent phase [34,65].

5.2.2. Terminus Retreat

Terminus retreat can increase glacier velocities [23], but this happens on interannual timescales rather than seasonal. Retreat can be triggered by thinning, which reduces friction at the glacier bed resulting in a velocity increase [24]. And indeed, thinning was observed on most of the glaciers during the study period with a mean elevation change of -1.59 ± 0.32 m a^{-1} (median: -0.94 ± 0.31 m a^{-1}) [15]. This also matches the finding that most of the glaciers retreated from 2015 to 2020. Retreat, however, was dominated by Columbia glacier, which retreated even further while splitting into separate glacier tongues and thinning annually by -3.20 ± 0.19 m [15].

Terminus retreat also depends on other conditions such as (1) whether the glacier tongue is grounded or not, (2) whether the terminus is buttressed by an ice mélange and (3) submarine melt [46]. (1) and (2) would need further investigation as this was beyond the scope of this study. (3) can be related from ocean temperature variation. Submarine melt either results from ambient melt due to warm ocean waters or from discharge driven melt where meltwater is discharged through the

 doi:10.20944/preprints202604.0745.v1

subglacial drainage system and forms plumes that enhance melt [26,60]. The latter is hypothesized to be the most important driver [16,26,60].

Jackson et al. [26] also state that submarine melt is the primary driver of terminus retreat during summer and glacier dynamics are the primary driver during winter. The observed strong negative correlation between ice discharge and ocean temperature (Figure 6) suggests a link between subglacial discharge and ice discharge. As ocean temperature decreases at the end of summer, ice discharge starts increasing again. When air and ocean temperature drop in fall, the subglacial channels change from efficient to inefficient, which leads to an increase in ice discharge [16,24].

The observed increasing trend in ocean temperature presumably elevates ambient melt. This might also partly explain the higher rate of terminus mass loss compared to Kochtitzky et al. [19]. The ocean temperature increase can be seen for most years and depths (Figure 7). Two years are the exception, 2017 and 2018, where temperatures are significantly lower between ~50 m and ~200 m depth. It is also notable that this difference is more pronounced for Yahtse (Figure 7d) than for Hubbard (Figure 7b) and Columbia (Figure 7c) glaciers. We observed this drop in mean ocean temperatures over the entire study region (Figure 8b).

5.2.3. Atmospheric Drivers

During the study period, the PDO index became increasingly more negative [66], coinciding with lower temperatures and precipitation (Figure 8). This might explain the decreasing trends for most of the analysed ERA5 variables, as a negative PDO phase is usually associated with lower temperatures and precipitation [11]. Short-term peaks in surface temperature and snowfall during 2015/2016 and 2018/2019 corresponded to El Niño events, while colder phases aligned with La Niña years [67]. These ENSO-driven variations also coincided with the ERA5 data, suggesting a considerable effect of ENSO on glacier mass balances in Alaska over the study period [45].

However, compared to previous studies in Alaska (Chapter 5.1), this does not seem to have impacted ice discharge. Surface temperature was weakly correlated (Figure 5a), but the comparison also reveals that ice discharge decrease happens shorty before surface temperatures reach a maximum in July. This means that the drainage system needs at least one or two months to develop, but once fully developed, it results in an ice discharge reduction of up to ~60%.

Precipitation had the lowest correlation of all variables and was not significant (Figure 5b). Snowfall showed no strong positive relationship (Figure 5d). The moderate negative correlation of rainfall might indicate efficient drainage during summer while ice discharge is low (Figure 5c). High amounts of rainfall, coinciding with an ice discharge increase during late summer, might indicate an accelerating effect from remaining summer rainfall in the drainage system [68]. This happens around August to October (Figure 5c) where ice discharge abruptly increases, also suggesting that the drainage system becomes inefficient again.

5.2.4. Glacier Geometry and Mass Balance

Compared to other regions and land terminating glaciers, marine-terminating glaciers in Alaska have experienced less mass loss [15]. A possible explanation is the coastal setting of these glaciers within high altitude, accompanied by high accumulation [34]. The response of a glacier, reflected in its mass balance, is determined by the glacier's geometry and the local climate variability [22]. Glacier geometry (width, surface and bed topography) is a first-order control on glacier dynamics [23,46].

Zeller et al. [69] recently published an inventory of accumulation area ratios (AAR) and equilibrium line altitudes (ELA) for over 3,000 glaciers in Alaska (88% of regional area) between 2018 and 2022. The study observed that maritime glaciers had lower ELAs compared to continental glaciers. ELAs were maximized during 2018 and 2019, which resulted from extraordinary high summer temperatures [69]. This was clearly coinciding with the observed rising temperatures on all marine-terminating glaciers during this study (Figure 8a).

 doi:10.20944/preprints202604.0745.v1

For regions with marine-terminating glaciers, Zeller et al. [69] reported greater surface elevation loss than for other regions with the same AAR. This might be due to mass loss from frontal ablation which cannot be constrained with AAR variability [19,69].

Many glaciers still had low ELAs and AARs >0.5 on average from 2018 to 2022. Glaciers with comparably low AAR are e.g., Turner glacier (AAR = 0.21), Northland glacier (AAR = 0.28) and First Branch Columbia glacier (AAR = 0.24).

Therefore, comparably low ice discharge values can be explained by such low AARs. Depending on glacier size and the sensitivity of ELA increase [70], glaciers with higher AAR ratios tend to show higher rates of ice discharge. This is especially the case for Hubbard glacier, which had the highest AAR (0.87) and the highest ice discharge of all glaciers (4.49 ± 1.30 Gt a^{-1}).

These findings show that in Alaska, increasingly negative surface mass balances and ice dynamics are the main reasons for mass loss [16]. Larsen et al. 2015 [22] demonstrated that marine-terminating glaciers contributed less to the mass loss in Alaska than land- or lake-terminating glaciers. It is believed that most marine-terminating glaciers have already slowed or stopped retreating, which would explain why the observed ice discharge is the primary contributor to frontal ablation [16].

6. Conclusions

This study provides a monthly series of ice discharge from marine terminating glaciers in Alaska. Ice discharge is combined with long-term terminus mass loss to give an estimate of the total frontal ablation over the same period. The mean yearly ice discharge rate of all glaciers from 2015 to 2021 was 11.81 ± 5.35 Gt a^{-1}. Hubbard glacier had the highest ice discharge with 4.49 ± 1.30 Gt a^{-1}. Glaciers also lost 1.30 ± 0.07 Gt a^{-1} due to terminus retreat, resulting in a total frontal ablation of 13.11 ± 5.35 Gt a^{-1}. Overall, ice discharge was the main contributor to frontal ablation accounting for 89%.

Seasonality in ice discharge of most glaciers (~89%) is likely controlled by the evolution of the subglacial drainage system. Most of the glaciers experienced a late summer decrease in ice discharge, which can be associated to a switch from an inefficient to an efficient drainage system. Maritime conditions with high amounts of snowfall and sufficient AARs might explain high rates of ice discharge. There was, however, a decreasing trend of precipitation and surface air temperature. Variability and trends of the ERA5 reanalysis data coincided with ENSO events and a switch from positive to negative PDO. Contrarily, ocean temperature still increased from 2015 to 2020.

Terminus mass loss only contributed ~11% to frontal ablation, which indicates that ambient melt from elevated ocean water temperature is not the primary driver for frontal ablation and that many glaciers possess quite stable front geometries. Although surface melt might have been less due to decreasing surface temperatures and rainfall, it is evident in most studies that surface melt is the main cause of glacier mass loss in Alaska.

Compared to other regions, marine-terminating glaciers in Alaska loose comparably low amounts by terminus mass loss. There were only a few cases where frontal ablation was elevated. Except for Columbia glacier, which experienced rapid retreat, most of the glaciers have already passed drastic terminus retreat.

The findings of this study aim to address the existing gap in frontal ablation estimates. The proposed methodology is adaptable to other regions and offers a systematic approach, facilitating the calculation of frontal ablation through ice discharge and terminus mass loss. Glacier surface mass balance observations or an automated glacier front detection could be implemented for more temporally detailed future studies. Further effort is needed to integrate the controlling mechanisms of retreat, e.g. subglacial topography and submarine melt.

Author Contributions: "Conceptualization, H.Z. and T.S.; methodology, H.Z. and D.P..; software, H.Z. and D.P.; formal analysis, H.Z..; data curation, H.Z. and D.P..; writing—original draft preparation, H.Z..; writing—review and editing, T.S. and D.P..; visualization, H.Z..; supervision, T.S..; project administration, T.S..; funding

 doi:10.20944/preprints202604.0745.v1

acquisition, T.S. All authors have read and agreed to the published version of the manuscript." Please turn to the CRediT taxonomy for the term explanation.

Funding: This research was funded by the Bayerisches Staatsministerium für Wissenschaft und Kunst within the Elite Network Bavaria with the Int. Doct. Program "Measuring and Modelling Mountain Glaciers in a Changing Climate" (IDP M3OCCA) as well as the German Research Foundation (DFG) project "Large-scale Automatic Calving Front Segmentation and Frontal Ablation Analysis of Arctic Glaciers using Synthetic-Aperture Radar ImageSequences (LASSI)" (grant numbers: CH 2080/5-1 and SE 3091/4-1) and the project "PAGE" within the DFG Emmy-Noether-Programme (grant number: SE 3091/5-1). We acknowledge financial support by Deutsche Forschungsgemeinschaft and Friedrich-Alexander-Universität Erlangen-Nürnberg within the funding program "Open Access Publication Funding".

Data Availability Statement: Data used within this analysis is publicly available at the respective resources listed in the manuscript.

Acknowledgments: During the preparation of this work, AI technologies were used to assist in the writing process. Specifically, ChatGPT(GPT-4) (OpenAI, San Francisco, CA, USA) was used in order to assist with rephrasing and improving readability. After using these tools, the manuscript was carefully reviewed, and the content was edited as needed. No tools or services were used for content generation.

Conflicts of Interest: "The authors declare no conflicts of interest.".

References

1. Copernicus Copernicus: 2023 Is the Hottest Year on Record, with Global Temperatures Close to the 1.5 °C Limit Available online: https://climate.copernicus.eu/copernicus-2023-hottest-year-record (accessed on 25 September 2024).
2. World Meteorological Organization (WMO) WMO Global Annual to Decadal Climate Update 2024-2028 2024.
3. NOAA 2023 Was the World's Warmest Year on Record, by Far | National Oceanic and Atmospheric Administration Available online: https://www.noaa.gov/news/2023-was-worlds-warmest-year-on-record-by-far (accessed on 25 September 2024).
4. Hock, R.; Rasul, G.; C. Adler, B. Cáceres, S. Gruber, Y. Hirabayashi, M. Jackson, A. Kääb, S. Kang, S. Kutuzov, Al. Milner, U. Molau, S. Morin, B. Orlove; Steltzer H. *High Mountain Areas. In: IPCC Special Report on the Ocean and Cryosphere in a Changing Climate [H.-O. Pörtner, D.C. Roberts, V. Masson-Delmotte, P. Zhai, M. Tignor, E. Poloczanska, K. Mintenbeck, A. Alegría, M. Nicolai, A. Okem, J. Petzold, B. Rama, N.M. Weyer (Eds.)]*; 1st ed.; Cambridge University Press, 2022; ISBN 978-1-009-15796-4.
5. Gardner, A.S.; Moholdt, G.; Cogley, J.G.; Wouters, B.; Arendt, A.A.; Wahr, J.; Berthier, E.; Hock, R.; Pfeffer, W.T.; Kaser, G.; et al. A Reconciled Estimate of Glacier Contributions to Sea Level Rise: 2003 to 2009. *Science* **2013**, *340*, 852–857, doi:10.1126/science.1234532.
6. Zemp, M.; Huss, M.; Thibert, E.; Eckert, N.; McNabb, R.; Huber, J.; Barandun, M.; Machguth, H.; Nussbaumer, S.U.; Gärtner-Roer, I.; et al. Global Glacier Mass Changes and Their Contributions to Sea-Level Rise from 1961 to 2016. *Nature* **2019**, *568*, 382–386, doi:10.1038/s41586-019-1071-0.
7. IPCC Climate Change 2021 – The Physical Science Basis: Working Group I Contribution to the Sixth Assessment Report of the Intergovernmental Panel on Climate Change; 1st ed.; Cambridge University Press, 2021; ISBN 978-1-009-15789-6.
8. Marzeion, B.; Jarosch, A.H.; Hofer, M. Past and Future Sea-Level Change from the Surface Mass Balance of Glaciers. *The Cryosphere* **2012**, *6*, 1295–1322, doi:10.5194/tc-6-1295-2012.
9. Zemp, M. *The Monitoring of Glaciers at Local, Mountain, and Global Scale*; Physische Geographie Glaziologie und Geomorphodynamik; Geographisches Inst. der Univ. Zürich: Zürich, 2012; ISBN 978-3-85543-261-5.
10. WGMS Global Glacier Change Bulletin No. 5 (2020–2021). Zemp, M., Gärtner-Roer, I., Nussbaumer, S.U., Welty, E.Z., Dussaillant, I. and Bannwart, J., (Eds.), ISC(WDS)/IUGG(IACS)/UNEP/UNESCO/ WMO, World Glacier Monitoring Service, Zurich, Switzerland, 134 Pp. 2023.

 doi:10.20944/preprints202604.0745.v1

11. Jakob, L.; Gourmelen, N.; Ewart, M.; Plummer, S. Spatially and Temporally Resolved Ice Loss in High Mountain Asia and the Gulf of Alaska Observed by CryoSat-2 Swath Altimetry between 2010 and 2019. *The Cryosphere* **2021**, *15*, 1845–1862, doi:10.5194/tc-15-1845-2021.
12. Millan, R.; Mouginot, J.; Rabatel, A.; Morlighem, M. Ice Velocity and Thickness of the World's Glaciers. *Nat. Geosci.* **2022**, *15*, 124–129, doi:10.1038/s41561-021-00885-z.
13. Marzeion, B.; Jarosch, A.H.; Hofer, M. Past and Future Sea-Level Change from the Surface Mass Balance of Glaciers. *The Cryosphere* **2012**, *6*, 1295–1322, doi:10.5194/tc-6-1295-2012.
14. Ciracì, E.; Velicogna, I.; Swenson, S. Continuity of the Mass Loss of the World's Glaciers and Ice Caps From the GRACE and GRACE Follow-On Missions. *Geophysical Research Letters* **2020**, *47*, e2019GL086926, doi:10.1029/2019GL086926.
15. Hugonnet, R.; McNabb, R.; Berthier, E.; Menounos, B.; Nuth, C.; Girod, L.; Farinotti, D.; Huss, M.; Dussaillant, I.; Brun, F.; et al. Accelerated Global Glacier Mass Loss in the Early Twenty-First Century. *Nature* **2021**, *592*, 726–731, doi:10.1038/s41586-021-03436-z.
16. McNabb, R.W.; Hock, R.; Huss, M. Variations in Alaska Tidewater Glacier Frontal Ablation, 1985–2013. *Journal of Geophysical Research: Earth Surface* **2015**, *120*, 120–136, doi:10.1002/2014JF003276.
17. Cogley, J.G.; Arendt, A.A.; Bauder, A.; Braithwaite, R.J.; Hock, R.; Jansson, P.; Kaser, G.; Moller, M.; Nicholson, L.; Rasmussen, L.A.; et al. Glossary of Glacier Mass Balance and Related Terms. **2010**.
18. Kochtitzky, W.; Copland, L. Retreat of Northern Hemisphere Marine-Terminating Glaciers, 2000–2020. *Geophysical Research Letters* **2022**, *49*, e2021GL096501, doi:10.1029/2021GL096501.
19. Kochtitzky, W.; Copland, L.; Van Wychen, W.; Hugonnet, R.; Hock, R.; Dowdeswell, J.A.; Benham, T.; Strozzi, T.; Glazovsky, A.; Lavrentiev, I.; et al. The Unquantified Mass Loss of Northern Hemisphere Marine-Terminating Glaciers from 2000–2020. *Nat Commun* **2022**, *13*, 5835, doi:10.1038/s41467-022-33231-x.
20. McNabb, R.W.; Hock, R. Alaska Tidewater Glacier Terminus Positions, 1948–2012. *Journal of Geophysical Research: Earth Surface* **2014**, *119*, 153–167, doi:10.1002/2013JF002915.
21. Post, A.; O'Neel, S.; Motyka, R.J.; Streveler, G. A Complex Relationship between Calving Glaciers and Climate. *Eos, Transactions American Geophysical Union* **2011**, *92*, 305–306, doi:10.1029/2011EO370001.
22. Larsen, C.F.; Burgess, E.; Arendt, A.A.; O'Neel, S.; Johnson, A.J.; Kienholz, C. Surface Melt Dominates Alaska Glacier Mass Balance. *Geophysical Research Letters* **2015**, *42*, 5902–5908, doi:10.1002/2015GL064349.
23. Enderlin, E.M.; O'Neel, S.; Bartholomaus, T.C.; Joughin, I. Evolving Environmental and Geometric Controls on Columbia Glacier's Continued Retreat. *Journal of Geophysical Research: Earth Surface* **2018**, *123*, 1528–1545, doi:10.1029/2017JF004541.
24. Vijay, S.; Braun, M. Seasonal and Interannual Variability of Columbia Glacier, Alaska (2011–2016): Ice Velocity, Mass Flux, Surface Elevation and Front Position. *Remote Sensing* **2017**, *9*, 635, doi:10.3390/rs9060635.
25. Burgess, E.W.; Larsen, C.F.; Forster, R.R. Summer Melt Regulates Winter Glacier Flow Speeds throughout Alaska. *Geophysical Research Letters* **2013**, *40*, 6160–6164, doi:10.1002/2013GL058228.
26. Jackson, R.H.; Motyka, R.J.; Amundson, J.M.; Abib, N.; Sutherland, D.A.; Nash, J.D.; Kienholz, C. The Relationship Between Submarine Melt and Subglacial Discharge From Observations at a Tidewater Glacier. *Journal of Geophysical Research: Oceans* **2022**, *127*, e2021JC018204, doi:10.1029/2021JC018204.
27. Recinos, B.; Maussion, F.; Rothenpieler, T.; Marzeion, B. Impact of Frontal Ablation on the Ice Thickness Estimation of Marine-Terminating Glaciers in Alaska. *The Cryosphere* **2019**, *13*, 2657–2672, doi:10.5194/tc-13-2657-2019.
28. Farinotti, D.; Huss, M.; Fürst, J.J.; Landmann, J.; Machguth, H.; Maussion, F.; Pandit, A. A Consensus Estimate for the Ice Thickness Distribution of All Glaciers on Earth. *Nat. Geosci.* **2019**, *12*, 168–173, doi:10.1038/s41561-019-0300-3.
29. Kienholz, C.; Hock, R.; Truffer, M.; Arendt, A.A.; Arko, S. Geodetic Mass Balance of Surge-Type Black Rapids Glacier, Alaska, 1980–2001–2010, Including Role of Rockslide Deposition and Earthquake Displacement. *Journal of Geophysical Research: Earth Surface* **2016**, *121*, 2358–2380, doi:10.1002/2016JF003883.
30. RGI 7.0 Consortium Randolph Glacier Inventory - A Dataset of Global Glacier Outlines, Version 7.0 2023.
31. RGI Randolph Glacier Inventory - A Dataset of Global Glacier Outlines, Version 6 2017.

 doi:10.20944/preprints202604.0745.v1

32. Davies, B.; McNabb, R.; Bendle, J.; Carrivick, J.; Ely, J.; Holt, T.; Markle, B.; McNeil, C.; Nicholson, L.; Pelto, M. Accelerating Glacier Volume Loss on Juneau Icefield Driven by Hypsometry and Melt-Accelerating Feedbacks. *Nat Commun* **2024**, *15*, 5099, doi:10.1038/s41467-024-49269-y.
33. Larsen, C.F.; Motyka, R.J.; Freymueller, J.T.; Echelmeyer, K.A.; Ivins, E.R. Rapid Viscoelastic Uplift in Southeast Alaska Caused by Post-Little Ice Age Glacial Retreat. *Earth and Planetary Science Letters* **2005**, *237*, 548–560, doi:10.1016/j.epsl.2005.06.032.
34. Burgess, E.W.; Forster, R.R.; Larsen, C.F. Flow Velocities of Alaskan Glaciers. *Nat Commun* **2013**, *4*, 2146, doi:10.1038/ncomms3146.
35. Schultz, J. *Die Ökozonen der Erde*; UTB Geowissenschaften, Ökologie, Agrarwissenschaften; 5., vollständig überarbeitete Auflage, Online-Ausgabe.; UTB GmbH: Stuttgart, 2016; ISBN 978-3-8252-4628-0.
36. Bieniek, P.A.; Bhatt, U.S.; Thoman, R.L.; Angeloff, H.; Partain, J.; Papineau, J.; Fritsch, F.; Holloway, E.; Walsh, J.E.; Daly, C.; et al. Climate Divisions for Alaska Based on Objective Methods. **2012**, doi:10.1175/JAMC-D-11-0168.1.
37. L'Heureux, M.L.; Mann, M.E.; Cook, B.I.; Gleason, B.E.; Vose, R.S. Atmospheric Circulation Influences on Seasonal Precipitation Patterns in Alaska during the Latter 20th Century. *Journal of Geophysical Research: Atmospheres* **2004**, *109*, doi:10.1029/2003JD003845.
38. Winski, D.; Osterberg, E.; Ferris, D.; Kreutz, K.; Wake, C.; Campbell, S.; Hawley, R.; Roy, S.; Birkel, S.; Introne, D.; et al. Industrial-Age Doubling of Snow Accumulation in the Alaska Range Linked to Tropical Ocean Warming. *Sci Rep* **2017**, *7*, 17869, doi:10.1038/s41598-017-18022-5.
39. Thoman, R.; McFarland, H.R. Alaska's Changing Environment 2.0. Alaska Center for Climate Assessment and Policy, International Arctic Research Center, University of Alaska Fairbanks. Uaf-Iarc.Org/Communicating-Change. **2024**.
40. Shahateet, K.; Navarro, F.; Seehaus, T.; Fürst, J.J.; Braun, M. Estimating Ice Discharge of the Antarctic Peninsula Using Different Ice-Thickness Datasets. *Annals of Glaciology* **2023**, *64*, 121–132, doi:10.1017/aog.2023.67.
41. Sánchez-Gámez, P.; Navarro, F.J. Ice Discharge Error Estimates Using Different Cross-Sectional Area Approaches: A Case Study for the Canadian High Arctic, 2016/17. *Journal of Glaciology* **2018**, *64*, 595–608, doi:10.1017/jog.2018.48.
42. Rott, H.; Müller, F.; Nagler, T.; Floricioiu, D. The Imbalance of Glaciers after Disintegration of Larsen-B Ice Shelf, Antarctic Peninsula. *The Cryosphere* **2011**, *5*, 125–134, doi:10.5194/tc-5-125-2011.
43. Hugonnet, R.; McNabb, R.; Berthier, E.; Menounos, B.; Nuth, C.; Girod, L.; Farinotti, D.; Huss, M.; Dussaillant, I.; Brun, F.; et al. Accelerated Global Glacier Mass Loss in the Early Twenty-First Century. *Nature* **2021**, *592*, 726–731, doi:10.1038/s41586-021-03436-z.
44. Friedl, P.; Seehaus, T.; Braun, M. Global Time Series and Temporal Mosaics of Glacier Surface Velocities Derived from Sentinel-1 Data. *Earth System Science Data* **2021**, *13*, 4653–4675, doi:10.5194/essd-13-4653-2021.
45. Hooke, R.LeB. *Principles of Glacier Mechanics*; 3rd ed.; Cambridge University Press: Cambridge, United Kingdom, 2020;
46. Catania, G.A.; Stearns, L.A.; Moon, T.A.; Enderlin, E.M.; Jackson, R.H. Future Evolution of Greenland's Marine-Terminating Outlet Glaciers. *Journal of Geophysical Research: Earth Surface* **2020**, *125*, e2018JF004873, doi:10.1029/2018JF004873.
47. Caldwell, N.G.; Armstrong, W.H.; McNabb, R.; Enderlin, E.M.; McGrath, D.; Rick, B.; Hanson, J.; Perry, L.B. Retreat and Frontal Ablation Rates for Alaska's Lake-Terminating Glaciers: Investigating Potential Physical Controls with Implications for Future Stability. *Journal of Glaciology* **2025**, 1–38, doi:10.1017/jog.2025.37.
48. Rasmussen, L.A.; Conway, H.; Krimmel, R.M.; Hock, R. Surface Mass Balance, Thinning and Iceberg Production, Columbia Glacier, Alaska, 1948–2007. *Journal of Glaciology* **2011**, *57*, 431–440, doi:10.3189/002214311796905532.
49. USGS Earth Explorer Available online: https://earthexplorer.usgs.gov/ (accessed on 2025 05-01).
50. Paul, F.; Barrand, N.E.; Baumann, S.; Berthier, E.; Bolch, T.; Casey, K.; Frey, H.; Joshi, S.P.; Konovalov, V.; Bris, R.L.; et al. On the Accuracy of Glacier Outlines Derived from Remote-Sensing Data. *Annals of Glaciology* **2013**, *54*, 171–182, doi:10.3189/2013AoG63A296.

 doi:10.20944/preprints202604.0745.v1

51. Mouginot, J.; Scheuchl, B.; Rignot, E. Mapping of Ice Motion in Antarctica Using Synthetic-Aperture Radar Data. *Remote Sensing* **2012**, *4*, 2753–2767, doi:10.3390/rs4092753.
52. Van Wychen, W.; Copland, L.; Gray, L.; Burgess, D.; Danielson, B.; Sharp, M. Spatial and Temporal Variation of Ice Motion and Ice Flux from Devon Ice Cap, Nunavut, Canada. *J. Glaciol.* **2012**, *58*, 657–664, doi:10.3189/2012JoG11J164.
53. Muñoz-Sabater, J.; Dutra, E.; Agustí-Panareda, A.; Albergel, C.; Arduini, G.; Balsamo, G.; Boussetta, S.; Choulga, M.; Harrigan, S.; Hersbach, H.; et al. ERA5-Land: A State-of-the-Art Global Reanalysis Dataset for Land Applications. *Earth System Science Data* **2021**, *13*, 4349–4383, doi:10.5194/essd-13-4349-2021.
54. ERA5-Land Monthly Averaged Data from 1950 to Present Available online: https://cds.climate.copernicus.eu/datasets/reanalysis-era5-land-monthly-means?tab=overview (accessed on 19 June 2025).
55. Dytham, C. *Choosing and Using Statistics : A Biologist's Guide*; Hoboken, NJ : Wiley-Blackwell, 2011; Vol. 3; ISBN 978-1-4051-9838-7.
56. Cleveland, R.B.; Cleveland, W.S.; Terpenning, I. STL: A Seasonal-Trend Decomposition Procedure Based on Loess. **1990**.
57. Lellouche, J.-M.; Greiner, E.; Bourdallé-Badie, R.; Garric, G.; Melet, A.; Drévillon, M.; Bricaud, C.; Hamon, M.; Le Galloudec, O.; Regnier, C.; et al. The Copernicus Global 1/12° Oceanic and Sea Ice GLORYS12 Reanalysis. *Frontiers In Earth Science* **2021**, *9*, doi:10.3389/feart.2021.698876.
58. Global Ocean Physics Reanalysis Available online: https://data.marine.copernicus.eu/product/GLOBAL_MULTIYEAR_PHY_001_030/description (accessed on 19 June 2025).
59. Lim, E.; Eakins, B.W.; Wigley, R. Coastal Relief Model of Southern Alaska: Procedures, Data Sources and Analysis Available online: https://www.ngdc.noaa.gov/mgg/coastal/s_alaska.html (accessed on 19 June 2025).
60. Jackson, R.H.; Nash, J.D.; Kienholz, C.; Sutherland, D.A.; Amundson, J.M.; Motyka, R.J.; Winters, D.; Skyllingstad, E.; Pettit, E.C. Meltwater Intrusions Reveal Mechanisms for Rapid Submarine Melt at a Tidewater Glacier. *Geophysical Research Letters* **2020**, *47*, e2019GL085335, doi:10.1029/2019GL085335.
61. Moon, T.; Joughin, I.; Smith, B.; van den Broeke, M.R.; van de Berg, W.J.; Noël, B.; Usher, M. Distinct Patterns of Seasonal Greenland Glacier Velocity. *Geophysical Research Letters* **2014**, *41*, 7209–7216, doi:10.1002/2014GL061836.
62. Yang, R.; Hock, R.; Kang, S.; Guo, W.; Shangguan, D.; Jiang, Z.; Zhang, Q. Glacier Surface Speed Variations on the Kenai Peninsula, Alaska, 2014–2019. *Journal of Geophysical Research: Earth Surface* **2022**, *127*, e2022JF006599, doi:10.1029/2022JF006599.
63. Stearns, L.A.; Hamilton, G.S.; van der Veen, C.J.; Finnegan, D.C.; O'Neel, S.; Scheick, J.B.; Lawson, D.E. Glaciological and Marine Geological Controls on Terminus Dynamics of Hubbard Glacier, Southeast Alaska. *Journal of Geophysical Research: Earth Surface* **2015**, *120*, 1065–1081, doi:10.1002/2014JF003341.
64. Armstrong, W.H.; Anderson, R.S.; Fahnestock, M.A. Spatial Patterns of Summer Speedup on South Central Alaska Glaciers. *Geophysical Research Letters* **2017**, *44*, 9379–9388, doi:10.1002/2017GL074370.
65. Trantow, T.; Herzfeld, U.C. Evolution of a Surge Cycle of the Bering-Bagley Glacier System From Observations and Numerical Modeling. *Journal of Geophysical Research: Earth Surface* **2024**, *129*, e2023JF007306, doi:10.1029/2023JF007306.
66. National Centers for Environmental Information. ERSST PDO Index 2025.
67. National Weather Service Climate Prediction Center. Cold & Warm Episodes by Season. Historical El Nino / La Nina Episodes (1950-Present) Available online: https://origin.cpc.ncep.noaa.gov/products/analysis_monitoring/ensostuff/ONI_v5.php (accessed on 5 July 2025).
68. Ing, R.N.; Nienow, P.W.; Sole, A.J.; Tedstone, A.J.; Mankoff, K.D. Minimal Impact of Late-Season Melt Events on Greenland Ice Sheet Annual Motion. *Geophysical Research Letters* **2024**, *51*, e2023GL106520, doi:10.1029/2023GL106520.

 doi:10.20944/preprints202604.0745.v1

69. Zeller, L.; McGrath, D.; Sass, L.; Florentine, C.; Downs, J. Equilibrium Line Altitudes, Accumulation Areas and the Vulnerability of Glaciers in Alaska. *Journal of Glaciology* **2025**, *71*, e28, doi:10.1017/jog.2024.65.
70. McGrath, D.; Sass, L.; O'Neel, S.; Arendt, A.; Kienholz, C. Hypsometric Control on Glacier Mass Balance Sensitivity in Alaska and Northwest Canada. *Earth's Future* **2017**, *5*, 324–336, doi:10.1002/2016EF000479.